Analysis of in vivo dynamics of influenza virus infection in mice using a GFP reporter virus

Balaji Manicassamy[a,b], Santhakumar Manicassamy[c], Alan Belicha-Villanueva[a,b], Giuseppe Pisanelli[a,d], Bali Pulendran[c], and Adolfo García-Sastre[a,b,e,1]

[a]Department of Microbiology, [b]Global Health and Emerging Pathogens Institute, and [e]Department of Medicine, Division of Infectious Diseases, Mount Sinai School of Medicine, New York, NY 10029; [c]Emory Vaccine Center, Emory University, Atlanta, GA 30329; and [d]Department of Pathology and Animal Health, School of Biotechnological Sciences, University of Naples "Federico II", 80137 Naples, Italy

Edited by Rafi Ahmed, Emory University, Atlanta, GA, and approved May 12, 2010 (received for review December 30, 2009)

Influenza A virus is being extensively studied because of its major impact on human and animal health. However, the dynamics of influenza virus infection and the cell types infected in vivo are poorly understood. These characteristics are challenging to determine, partly because there is no efficient replication-competent virus expressing an easily traceable reporter gene. Here, we report the generation of a recombinant influenza virus carrying a GFP reporter gene in the NS segment (NS1-GFP virus). Although attenuated when compared with wild-type virus, the NS1-GFP virus replicates efficiently in murine lungs and shows pathogenicity in mice. Using whole-organ imaging and flow cytometry, we have tracked the dynamics of influenza virus infection progression in mice. Imaging of murine lungs shows that infection starts in the respiratory tract in areas close to large conducting airways and later spreads to deeper sections of the lungs. In addition to epithelial cells, we found GFP-positive antigen-presenting cells, such as $CD11b^{+}CD11c^{-}$, $CD11b^{-}CD11c^{+}$, and $CD11b^{+}CD11c^{+}$, as early as 24 h after intranasal infection. In addition, a significant proportion of NK and B cells were GFP positive, suggesting active infection of these cells. We next tested the effects of the influenza virus inhibitors oseltamivir and amantadine on the kinetics of in vivo infection progression. Treatment with oseltamivir dramatically reduced influenza infection in all cell types, whereas, surprisingly, amantadine treatment more efficiently blocked infection in B and NK cells. Our results demonstrate high levels of immune cells harboring influenza virus antigen during viral infection and cell-type–specific effects upon treatment with antiviral agents, opening additional avenues of research in the influenza virus field.

antivirals | pathogenesis | recombinant influenza virus | GFP virus | cell tropism

Influenza A virus (IAV), a member of the *Orthomyxoviridae* family, causes respiratory disease that can be very severe, especially in very young children and elderly individuals (1). Apart from yearly seasonal outbreaks, IAV can cause frequent epidemics and occasional pandemics in humans (2, 3). Vaccination has been one of the most effective means of protection against influenza virus infection. In addition, there are two categories of Food and Drug Administration-approved drugs used for treatment of IAV infections: (*i*) M2 inhibitors, which block viral uncoating and entry (amantadine and rimantadine); and (*ii*) NA inhibitors, which block viral spreading (oseltamivir and zanamivir; reviewed in refs. 4–7).

Although studies on IAV using animal models and tissue culture have provided tremendous knowledge about both the viral and host factors that determine pathogenesis, following viral infection in vivo may provide us with a more complete picture of the complex interactions between the virus and the host (8). Such in vivo studies have been hampered primarily due to the lack of fully virulent IAV-expressing reporter genes that can be easily detected in vivo. Previous studies have attempted to create replication competent IAV viruses carrying a GFP reporter gene by replacing portions of the NS1 or the NA segments with GFP (9, 10). However, most of these viruses have reduced levels of replication and do not show significant pathogenesis in mice (9). Therefore, a number of basic questions related to IAV infection progression in vivo, and the extent to which different cell types are infected by the virus in the respiratory tract, remain unanswered.

In this study, using reverse genetics, we have generated a recombinant IAV carrying a GFP reporter in the NS segment (NS1-GFP virus). This work describes the successful generation of a mouse-lethal IAV virus expressing a fluorescent protein. Despite some levels of attenuation, the NS1-GFP virus replicates efficiently in eggs, Madin–Darby canine kidney (MDCK) cells, and in murine lungs. We characterized the in vivo dynamics of IAV infection progression in mice and identified different cell types that are susceptible to influenza virus infection. Whole-organ imaging of NS1-GFP virus–infected lungs was consistent with IAV infections starting in the respiratory tract near the trachea and main stem bronchi, spreading with time into bronchioles. Also, we have tested two well-known antiviral agents, amantadine and oseltamivir, which block virus uncoating and virus spreading, respectively. By visualizing the in vivo targets of IAV infection and the dynamics of infection progression, we are likely to gain a better understanding of IAV pathogenesis. In addition, a replication-competent IAV expressing GFP can serve as an important tool to more precisely analyze the impact in vivo of different vaccine strategies, immune modulators, and antiviral agents against IAV.

Results

Generation of IAV Expressing GFP. The NS segment of IAV encodes two proteins: NS1 produced from unspliced mRNA, and NEP produced from spliced mRNA (Fig. 1*A*). It has been previously shown that functionally active NS1 and NEP can be expressed as a single polyprotein with a foot and mouth disease virus (FMDV) 2A autoproteolytic cleavage site (11). During translation, the NS1 protein is separated from NEP by the cleavage of site 2A. In this study, we modified the NS segment to express NS1-GFP and NEP as a single polyprotein with a 19aa porcine teschovirus–1 (PTV-1) 2A autoproteolytic cleavage site between them, allowing NEP to be released from the upstream NS1-GFP protein during translation (11, 12). Also, we introduced two silent mutations in the splice acceptor site to prevent splicing of NS mRNA (11). The NS1-GFP virus was rescued using standard reverse genetics techniques as previously described (13). Although the initial rescue supernatant contained a mixture of both GFP-positive and GFP-negative virus populations, we were able to isolate a stable

Author contributions: B.M., S.M., A.B.-V., G.P., B.P., and A.G.-S. designed research; B.M., S.M., A.B.-V., and G.P. performed research; B.M., B.P., and A.G.-S. contributed new reagents/analytic tools; B.M., S.M., A.B.-V., G.P., B.P., and A.G.-S. analyzed data; and B.M., S.M., and A.G.-S. wrote the paper.

Conflict of interest statement: Mount Sinai School of Medicine has filed a patent application covering the use of recombinant influenza viruses expressing a reporter gene.

This article is a PNAS Direct Submission.

Freely available online through the PNAS open access option.

[1]To whom correspondence should be addressed. E-mail: adolfo.garcia-sastre@mssm.edu.

This article contains supporting information online at www.pnas.org/lookup/suppl/doi:10.1073/pnas.0914994107/-/DCSupplemental.

MICROBIOLOGY

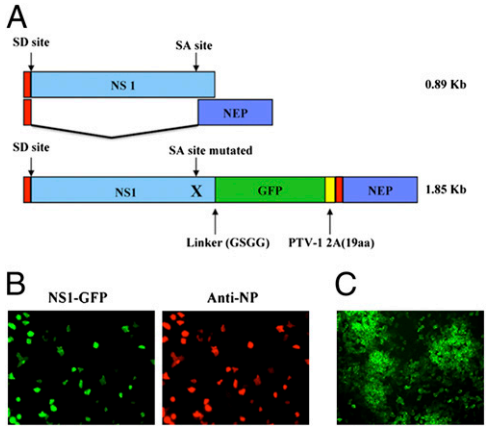

Fig. 1. Generation of recombinant influenza virus carrying a GFP reporter. (*A*) Schematic representation of NS segment of WT PR8 virus and NS1-GFP virus. Splice acceptor site in NS was mutated to prevent mRNA splicing (SD- splice donor site, SA- splice acceptor site). Common regions present in both NS1 (light blue) and NEP (dark blue) are shown in red. NS1was fused to GFP (green) via a GSGG linker, followed by PTV-1 2A autproteolytic cleavage site (yellow) and NEP ORF (red-blue). (*B*) A549 cells were infected with recombinant PR8 virus carrying NS1-GFP. At 10 hpi, cells were fixed and stained for NP. NP staining is shown in red and NS1-GFP is shown in green. (*C*) Fluorescent micrographs of NS1-GFP virus plaques taken at 20× magnification.

GFP carrying clone after three rounds of plaque purification. To test whether GFP was expressed in all infected cells, A549 cells were infected with the NS1-GFP virus at a MOI of 1 and stained for the viral nucleoprotein (NP), a viral protein critical for replication (Fig. 1*B*). At 10 h postinfection (hpi), NS1-GFP expression was observed in all cells expressing NP (infected cells), demonstrating that GFP is expressed in all infected cells (Fig. 1*B*). In addition, NS1-GFP virus was capable of undergoing multiple rounds of replication, formed visible GFP-expressing plaques (Fig. 1*C*), and grew to titers of 5×10^8 pfu/mL in 9-d-old embryonated eggs. The quality of the NS1-GFP virus preparation was further determined by examining GFP expression in 20 randomly selected visible plaques. Only preparations in which all 20 plaques were GFP positive were used in our experiments.

In Vitro Characterization of NS1-GFP Virus. ***NS1-GFP virus replicates in MDCK cells.*** To test whether the presence of a longer NS segment in NS1-GFP virus, which is approximately twice the size of the wild-type PR8 (WT PR8) NS segment (1.89 kb vs. 0.89 kb), affects the virus replication cycle in tissue culture, we compared the growth kinetics of NS1-GFP virus and parental virus WT PR8 in MDCK cells (Fig. S1*A*). MDCK cells were infected with either NS1-GFP or WT PR8 virus at MOI of 1 or of 0.001, and at various time points postinfection the viral titers in the supernatant were quantified by plaque assay. In a single-cycle replication assay (MOI = 1), NS1-GFP virus showed growth patterns similar to those of WT PR8 virus, with titers reaching up to 2×10^7 pfu/mL However, in a multicycle replication assay (MOI = 0.001), NS1-GFP virus showed a slight delay in replication kinetics, with titers reaching up to 4×10^5 pfu/mL. This indicates that NS1-GFP virus can undergo multicycle replication in MDCK cells, albeit reaching ≈100-fold lower titers than WT virus.

Next, the NS1 protein expression profile was examined in infected MDCK cells by Western blot analysis (Fig. S1*B*). In the WT PR8-infected cells, NS1 expression can be seen as early as 6 hpi. In NS1-GFP virus–infected cells, NS1-GFP expression could be detected at the earliest by 8 hpi, suggesting a modest delay in NS1-GFP expression.

NS1-GFP virus suppress IFN-β promoter activation. A well-characterized function of IAV NS1 protein is the suppression of IFN-β promoter induction via IRF-3 activation (14). We therefore examined whether this antagonist function of NS1 is intact in the NS1-GFP virus. MDCK cells stably expressing firefly luciferase under the control of the IFN-β promoter were infected with either WT PR8 or NS1-GFP virus at a MOI of 1. An IAV carrying a deletion of NS1 (WSN ΔNS1) was used as a positive control. The cell lysates were analyzed for firefly luciferase activity at 18 hpi as an indirect quantification of IFN-β promoter activity. The luciferase activity in NS1-GFP virus–infected cells is similar to that in PR8-infected cells, suggesting that the NS1-GFP virus is capable of blocking IFN-β induction as efficiently as WT PR8 NS1 (Fig. S1*C*). In contrast, WSN ΔNS1 virus, which lacks the ability to block IFN-β induction, in infected cells showed nearly a 1,200-fold activation of IFN-β promoter. These results show that the NS1-GFP virus is competent in blocking the induction of IFN-β promoter during IAV infection.

In Vivo Characterization of NS1-GFP Virus. ***NS1-GFP virus causes significant pathogenicity in mice.*** WT PR8 has been previously shown to cause severe pathogenicity in mice (11, 15). To test whether the NS1-GFP virus is comparable in disease induction to its parental virus, BALB/c mice were infected intranasally with either NS1-GFP or WT PR8 virus at different doses, and body weight loss and survival were measured (Fig. 2 *A* and *B* and Fig. S2). In the WT PR8-infected mice, all mice infected with a dose 10^2 pfu or higher showed significant weight loss starting 2 dpi, and all mice succumbed to infection by day 10 (Figs. S2*A* and 2*A*). In the NS1-GFP virus–infected mice, only mice that received 10^4 pfu or higher showed significant weight loss, and all of them lost more than 25% body weight by day 9 and were humanely killed (Figs. S2*B* and 2*B*). This indicates that NS1-GFP virus is attenuated compared with PR8 virus. Based on the survival data, we determined the LD_{50} value for NS1-GFP virus as 3,160 pfu, ~100-fold higher than parental PR8 virus (31.60 pfu) (16). Despite the attenuation of the NS1-GFP virus in vivo, it is still possible to use a lethal dose of this virus in the murine model.

We then examined the viral titers in the lungs of infected mice on day 3 and day 4 postinfection (Fig. 2*C*). The NS1-GFP virus replicated efficiently in the lower respiratory tract of mice and grew to nearly 5×10^6 pfu/mL, only 2-fold lower than WT PR8 virus. This slight reduction in replication is likely to account for the increase in LD_{50}.

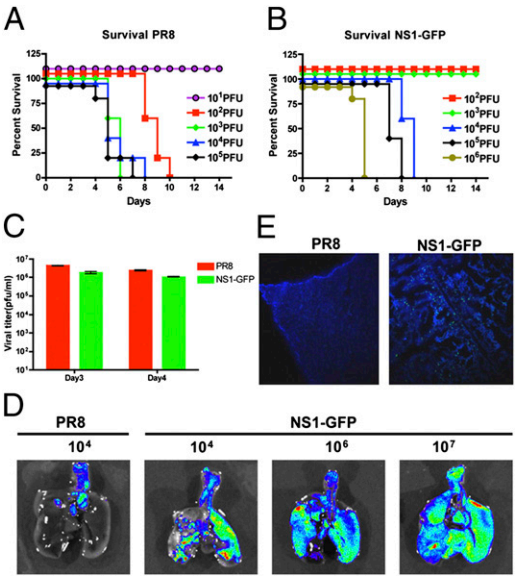

Fig. 2. In vivo characterization of NS1-GFP virus. (*A* and *B*) Comparison of survival of PR8 and NS1-GFP virus–infected mice. BALB/c mice were intranasally inoculated with indicated doses of PR8 or NS1-GFP virus. Survival was monitored daily. (*C*) Viral titers in lungs of mice infected with WT PR8 virus and with NS1-GFP viruses. (*D*) Mice were intranasally inoculated with either PR8 or NS1-GFP virus at indicated doses. Lungs were excised on day 4 postinfection, and fluorescence from infected lungs was imaged using an IVIS-200 imaging system (Xenogen). (*E*) Fluorescent micrographs of mice lung cryosections (10× magnification).

Whole-organ imaging of NS1-GFP virus replication. To longitudinally follow the course of infection progression in the lungs of infected mice, we imaged the NS1-GFP virus–infected mice using an IVIS-200 series system (Xenogen). Five-wk-old BALB/c mice were infected with WT PR8 (10^4 pfu) or NS1-GFP virus with different doses (10^4, 10^6, and 10^7 pfu). WT PR8-infected mice were used as controls for background fluorescence. Unfortunately, we found that background fluorescence from skin and tissues surrounding the rib cage precluded us from an in-depth analysis of GFP expression in the lung of anesthetized mice following virus infection. To overcome this, animals were killed and their lungs were excised and imaged ex vivo on day 4 postinfection (Fig. 2*D*). Upon viral infection, the level of fluorescence from the lungs of NS1-GFP virus–infected mice was significantly higher than in WT PR8-infected mice (background), indicating active replication of NS1-GFP virus in the lower respiratory tract of infected mice (Fig. 2*D*). We observed a good correlation between the amount of viral inoculum and the fluorescence signal from NS1-GFP virus–infected lungs, with fluorescence intensity increasing as the dose of the inoculum increased. Furthermore, examination of cryosections of NS1-GFP virus–infected lungs also showed infected cells expressing NS1-GFP protein (Fig. 2*E*).

Kinetics of NS1-GFP Virus Infection in Mice. Previous studies have shown that IAV infects both epithelial ($CD45^-$) and hematopoietic ($CD45^+$) cells in vitro (8, 17–20). To better understand the in vivo dynamics of IAV infection progression, and to identify the specific cell types susceptible to IAV infection, BALB/c mice were infected with NS1-GFP virus and then analyzed for GFP-positive cells in lung homogenates using multicolor flow cytometry. Representative plots of the flow-cytometric analysis of GFP in different cell types are shown in Figs. S3 and S4.

To find the optimal viral dose that would allow us to follow the kinetics of infection, mice were infected intranasally with NS1-GFP virus at different doses (10^4, 10^6, and 10^7 pfu), and the course of infection of nonhematopoietic cells ($CD45^-$) was analyzed at different times postinfection (Fig. 3*A*). Flow cytometry analysis of lung cells showed an increase in the number of infected cells as the NS1-GFP viral inoculum increased, correlating well with the results from ex vivo imaging. In the 10^7 pfu-infected mice, GFP-positive cells could be seen as early as 12 hpi, with nearly 6% of $CD45^-$ cells being GFP positive, and these infection levels remained sustained up to 72 hpi. At 96 hpi, the number of GFP-positive cells decreased by nearly 3-fold. The 10^6 pfu-infected group showed a kinetic pattern of GFP-positive cells with numbers peaking around 48–72 hpi at levels similar to the 10^7 pfu-infected group. However, in the 10^4 pfu-infected mice, despite showing severe pathogenicity, only 1% of $CD45^-$ cells were GFP positive (2- to 3-fold higher than background levels; Fig. 3*A*). Based on these data, the subsequent experiments were performed with a dose of 10^6 pfu.

We next examined the expression of NS1-GFP in various subsets of antigen presenting cells (APC) based on the surface expression patterns of CD11b and CD11c. Mice were intranasally inoculated with 10^6 pfu of NS1-GFP virus, and the lung homogenates were analyzed for GFP presence in APCs using antibodies specific for CD11b and CD11c surface markers at 12, 24, 48, 72, and 120 hpi (Fig. 3*B*). At 12 hpi, we observed a minimal number of cells expressing NS1-GFP (<1%). However after 24 hpi, the number of GFP containing cells increased. At 48 hpi, nearly 10% of the $CD11b^+$ $CD11c^+$ (conventional DCs) and $CD11b^+$ $CD11c^-$ (monocytes and neutrophils) cells were carrying NS1-GFP. At this time only 2–3% of $CD11b^-$ $CD11c^+$ (macrophages and dendritic cells) were GFP positive. After 96 hpi, the numbers of GFP-positive cells started to decline, and only $CD11b^+$ $CD11c^+$ cells carried significantly higher levels of NS1-GFP (~6%). In addition, a significant percentage of NK and B cells were also GFP positive, suggesting that these cells are targets of IAV infection (Fig. 4; No treatment). We also found a minor portion of CD4 and CD8 cells carrying GFP (Fig. 4; No treatment). Although macrophages, DC, and monocytes are known to be susceptible to IAV infection in vitro, it is possible that, in vivo, some of these cells are GFP positive due to uptake of NS1-GFP virus–infected cells or from apoptotic cells (17–23).

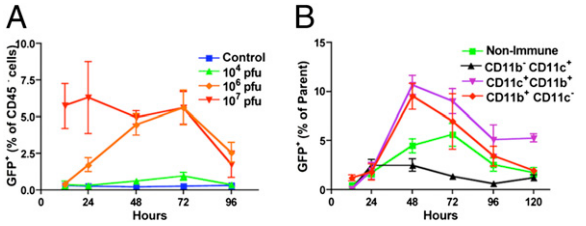

Fig. 3. Dynamics of influenza virus infection in lungs. (*A*) Kinetics of epithelial cell infection. BALB/c mice were intranasally inoculated with NS1-GFP virus at indicated doses, and lung homogenates were analyzed for GFP expression in nonhematopoietic cells ($CD45^-$) using a BD LSR II flow cytometer. (*B*) Comparison of kinetics of hematopoietic and nonhematopoietic cell infection in murine lungs. BALB/c mice were intranasally inoculated with 10^6 pfu NS1-GFP virus and analyzed for GFP expression in cells types differentially expressing CD11b and CD11c. Each data point represents the average from at least three mice.

Effects of Antiviral Treatments on NS1-GFP Infection Progression. Although vaccination is the most effective means of protection against lethal influenza virus infection, antiviral drugs such as amantadine and oseltamivir are recommended for treatment of influenza-like illnesses (4, 5). The mechanisms of action of these drugs have been extensively studied in tissue culture. However, it is unclear how these drugs modulate the progression of viral infection in vivo. To understand how antiviral treatment affects the kinetics of virus infection, mice were infected with 10^6 pfu of NS1-GFP virus, and were treated daily with either amantadine (40 mg/kg) or oseltamivir (50 mg/kg) starting 1 h after infection (24). The effect of antiviral treatments was determined by analyzing NS1-GFP expression in different cells types using multicolor flow cytometry (Fig. 4). In mice that received no antiviral drug, we observed a differential kinetic pattern of NS1-GFP expression in different cell types with the numbers of GFP-positive cells peaking at 48–72 hpi. Oseltamivir treatment dramatically reduced the infection rate in all of the examined cell types. We were able to detect only modest levels of GFP positive cells in all cell types (>2%). Interestingly, amantadine treatment was most effective in blocking infection of NK and B cells, but was less potent for other cell types (Fig. 4 *F* and *G*). Amantadine treatment showed only a 50% reduction in infection of epithelial ($CD45^-$) and $CD11b^+$ $CD11c^+$ cells (Fig. 4 *A* and *C*). This drug was effective in reducing the numbers of GFP-positive cells in $CD11b^+$ $CD11c^-$, $Gr1^+$ (infiltrating monocytes) and CD4 cells at early times but not after 72 hpi (Fig. 4 *D, E,* and *H*). Taken together, these results show that oseltamivir treatment controls infection progression in all cell types but that amantadine blocks infection in a more cell type-specific manner.

To observe the global effects of oseltamivir treatment, ex vivo analysis of whole lungs was performed (Fig. 5). Lungs from noninfected mice were used as controls for background fluorescence. Analysis of mice lungs on day 2 postinfection showed a clear difference in the fluorescence intensities between untreated mice and oseltamivir-treated mice (Fig. 5*A*). In both groups, most of the GFP fluorescence signal was concentrated in areas close to large conducting airways. However, fluorescence intensity was significantly lower in oseltamivir-treated mice than in untreated mice (3- to 5-fold lower). Analysis of the untreated group on day 4 postinfection showed GFP fluorescence throughout the whole lung, demonstrating the progression of infection into the lungs (Fig. 5*B*). However, oseltamivir treatment significantly restricted the spread of viral infection, as the GFP signal was detected only in localized spots. Together, our data indicate that oseltamivir treatment greatly reduces IAV infection in both epithelial and immune cells,

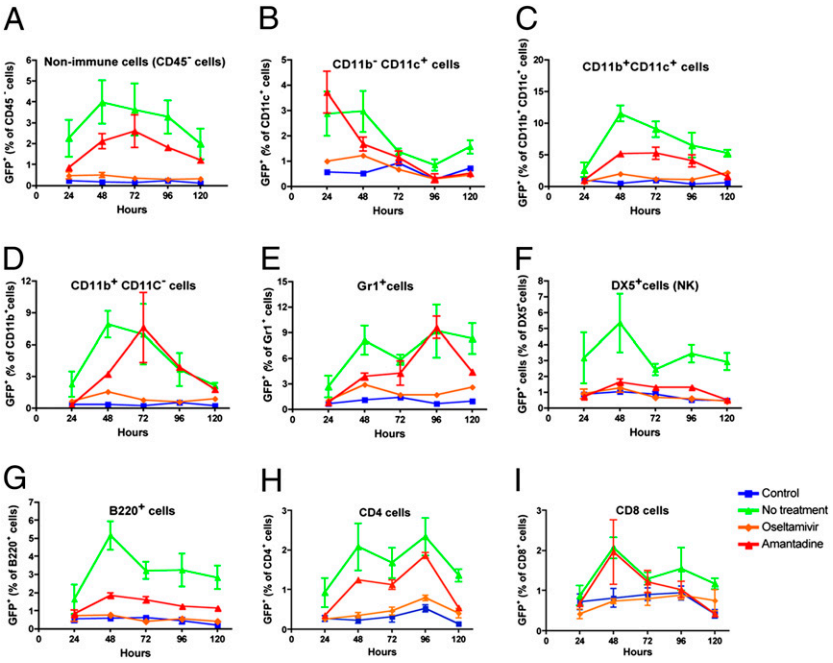

Fig. 4. Oseltamivir and amantadine treatment significantly reduces NS1-GFP virus infection. Mice infected with NS1-GFP virus either were left untreated or were treated with oseltamivir (50 mg/kg) or amantadine (40 mg/kg), starting 1 h postinfection. Kinetics of infection progression in different cell types were analyzed using a BD LSR II flow cytometer. (*A*–*G*) Kinetics of GFP expression in different cell types as indicated in treated and untreated groups.

and that infection is restricted to small localized areas in the lung, which may represent the initial sites of infection.

In Vivo and in Vitro Stability of GFP Expression by NS1-GFP Virus. Although NS1-GFP virus replicated in mice, in the lung homogenates, we observed a mixture of GFP-positive and GFP-negative viruses, suggesting that some of the viruses may carry deletions in the GFP transgene. To fully evaluate the in vivo stability of NS1-GFP virus, mice were infected with 10^4 pfu of NS1-GFP virus, and the percentages of GFP carrying virus in the lung homogenates were assessed on days 2, 4, and 6 by scoring for GFP-positive or GFP-negative plaques (Fig. S5*A*). The viral stocks used for murine infection served as controls. The percentage of GFP-positive and GFP-negative plaques varied among individual mice. We observed that nearly 15% plaques were GFP negative in the day-2 and day-4 lung homogenates. However, in the lung homogenates from day 6 postinfection, nearly 30% of plaques were GFP negative, suggesting increased loss of GFP or active replication of GFP deletion viruses. To assess the kinetics of stability of GFP transgene in mice, we compared GFP expression with viral nucleoprotein NP expression in nonimmune cells ($CD45^-$) in mice infected with 10^6 pfu NS1-GFP virus. Unlike immune cells that can carry GFP by phagocytosis of infected cells, nonimmune cells will carry GFP only if they are infected. At 24 hpi, the percentage of NP^+ cells was twice the percentage of GFP^+ cells (Fig. S5*B*). At this time during infection, the higher number NP^+ cells is unlikely from the emergence of GFP deletion virus but rather the early expression of NP compared with NS1-GFP. During the course of infection, both populations followed similar kinetic patterns. This correlates with the plaque assay data showing that a majority of the virus population carry GFP (Fig. S5*A*).

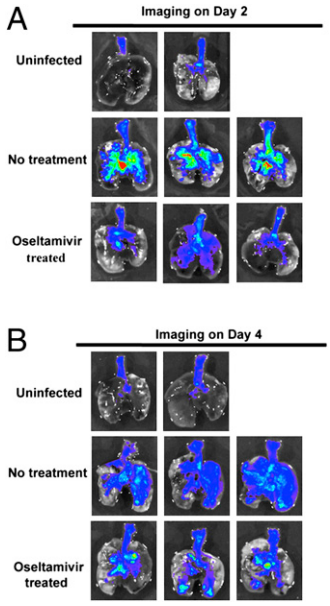

Fig. 5. Oseltamivir treatment restricts influenza virus infection to localized areas. Ex vivo imaging of mice lungs on day 2 (*A*) and day 4 (*B*) postinfection. BALB/c mice infected with NS1-GFP virus (10^6 pfu) either were left untreated or were treated daily once with oseltamivir (50 mg/kg). Lungs of mice were excised at indicated time and imaged using the IVIS-200 system (Xenogen).

We next examined the stability of NS1-GFP virus in vitro during a multicycle replication in MDCK cells. MDCK cells were infected with an MOI of 0.001, and the levels of GFP-positive and GFP-negative viruses in the supernatants were examined by plaque assay at various hpi (Fig. S5*C*). At 12 hpi, we observed that nearly 5–10% of plaques were GFP negative. During multicycle replication, the number of GFP-negative viruses increased from 25% to 45%, suggesting better growth of viruses carrying deletions in GFP gene. Nevertheless, it is possible to generate clonal populations of the NS1-GFP virus from single plaques with more than 99% of GFP-positive viruses.

Discussion

In this study, we report the generation of a fully replication competent influenza GFP reporter virus. The NS1-GFP virus was attenuated for multicycle replication in MDCK cells and in mice. Nevertheless, the NS1-GFP virus was still pathogenic in mice. This phenotype allowed us to monitor the virus-infected cells in vivo using a fluorescent reporter gene during infection with a lethal dose of influenza virus. Whole-organ imaging of lungs of mice infected with NS1-GFP virus was consistent with influenza virus infection, starting in the large conducting airways and later spreading to the bronchioles and deeper areas in the lungs. Although there was background fluorescence in the large conducting airways of noninfected mice, the fluorescence intensity in the large conducting airways of NS1-GFP virus–infected

mice (ROI intensity, 203.50 ± 41.36) was nearly 2-fold higher than in the noninfected mice (ROI intensity, 108.39 ± 14.56). We also analyzed the in vivo dynamics of IAV infection by flow cytometry, and found that GFP is present in epithelial and hematopoietic cells including macrophages, monocyte, neutrophils, respiratory dendritic cells, B, NK, CD4, and CD8 cells. Treatment of mice with a NA inhibitor dramatically reduced virus spreading to all cell types. However, treatment with an M2 inhibitor effectively reduced infection of B and NK cells, but showed only a modest effect in blocking infection of other cells, suggesting that B and NK cells are more susceptible to the antiviral action of amantadine. This differential susceptibility of cell populations in vivo to the antiviral effects of two different influenza virus drugs is likely to have implications for control of disease progression and the induction of immune responses.

In our NS1-GFP virus, the GFP reporter was introduced in the middle of the NS segment to prevent any detrimental effect on vRNA packaging signals present in the 3′ and 5′ ends. Previously, Kittel et al. and Shinya et al. generated IAV carrying GFP by replacing portions of NS or NA segment with GFP, respectively (9, 10). However, these viruses were highly attenuated in cell culture and mice. We have designed the NS1-GFP virus to express NS1-GFP and NEP as a single fusion protein (NS1-GFP-2A-NEP), building on a strategy previously described by our group (Fig. 1*A*) (11). NEP, which is essential for virus survival, is separated from NS1-GFP protein by an autoproteolytic cleavage reaction at 2A site.

In mice, the NS1-GFP virus caused significant pathogenicity, evidenced by significant loss of body weight and by 100% lethality at doses $\geq 10^4$ pfu (Fig. 2*B* and Fig. S2*B*). All of the mice infected with 10^4 pfu of NS1-GFP virus reached the experimental end point by day 9. Also, NS1-GFP virus replicated efficiently in the lower respiratory tract of infected mice (Fig. 2*C*). Interestingly, we did notice nearly 5–30% of the GFP-negative viruses in the murine lung homogenates, indicating that these viruses are likely carrying deletions in the GFP (Fig. S5*A*). In our multiple analyses of NS1-GFP virus stocks, we did not find GFP-negative plaques (limit, >10 pfu). The GFP-negative viruses may arise due to selection pressure for viruses that contain deletions or mutations at specific regions of the NS-GFP segment that result in more fit viruses in vivo. This is in contrast to nonsegmented, negative strand RNA viruses, which are known to stably maintain GFP and other reporter genes inserted in their genomes after multiple passages (25). Nevertheless, as nearly 70% of the virus population in the lungs of infected animals remained GFP positive (day 6), we do not believe that our analysis has been highly compromised by loss of GFP expression during infection.

Previous studies have shown that IAV preferentially replicate in tracheal epithelial cells (8, 26). We analyzed the sites of initial viral replication and the spreading from these sites in the murine model by performing whole-organ imaging of NS1-GFP–infected lungs. Ex vivo imaging of NS1-GFP virus–infected lungs revealed that GFP fluorescence signal was present mainly in areas closer to large conducting airways during the initial stages of infection, suggesting active replication of the NS1-GFP virus in this region (Fig. 5*A,* No treatment). At later stages of infection, GFP signal could be seen throughout the lung, indicating the spreading of NS1-GFP virus deeper into the bronchioles and possible into the alveoli spaces (Fig. 5*B,* No treatment; Fig. 2*D*). Treatment of infected mice with oseltamivir effectively blocked viral spreading, and NS1-GFP virus replication was observed in confined regions in the lungs. This is in agreement with the data from in vitro studies that have demonstrated that oseltamivir restricts viral spreading by blocking release of progeny virions from the infected cells (reviewed in ref. 4). It is important to note that sites of IAV replication and viral spreading in lungs are determined by several viral/host factors, including the origin of virus (avian or human), the hemagglutination receptor specificity, distribution of susceptible cells, sialic acid receptor distributions, and temperature (27, 28). It has been proposed that these factors contribute to impaired human-to-human transmission of highly pathogenic H5N1 virus (29). Thus, recombinant influenza viruses expressing NS1-GFP and derived from different strains might be used to address these questions in different animal models.

Flow-cytometric analysis of infected lung homogenates revealed the kinetics of IAV infection in different cell types. Mice were infected with different doses (10^4, 10^6, or 10^7 pfu) of NS1-GFP virus, and the infection progression was followed in different cell types. In the 10^7-pfu group, during the early stages of infection, GFP expression was seen mostly in nonimmune $CD45^-$ cells (12–24 hpi), indicating that these cells are the primary targets of IAV infection, and only after 24 hpi was GFP expression detected in hematopoietic cells (Fig. 3). The percentage of GFP-positive epithelial cells remained nearly 6% from 12 to 72 hpi. However, in mice infected with 10^6 pfu, a kinetic pattern of infection progression was observed. The number of infected cells in different cell types remained at less than 1% at 12 hpi but increased over time, reaching a peak at 48–72 hpi. We observed a distinct pattern of susceptibility to infection by the NS1-GFP virus for different immune cells in the following order: $CD11b^+$ $CD11c^+$ > $Gr1^+$ ≥ $CD11b^+$ $CD11c^-$ > $CD11b^-$ $CD11c^+$. NS1-GFP was also present in B, NK, CD4, and CD8 cells (Fig. 4). At 72 hpi, the number of GFP-positive cells declined, probably due to clearance of infected cells by the immune system and to migration of DCs to draining lymph nodes. It is worthwhile noting that some of these cells actively take up foreign antigen and cell debris, so it is possible that some these cells are not infected but, rather, carry the debris of infected cells (30). Because of technical limitations, we were unable to differentiate between cells directly infected with NS1-GFP virus and cells carrying infected-cell debris.

Several studies have shown that highly pathogenic viruses such as the 1918 H1N1 virus and H5N1 viruses induce massive infiltration of inflammatory cells (monocytes and neutrophils) very early during infection, and that these viruses can replicate efficiently in these cells (31–33). In addition, mice infected with highly pathogenic H5N1 viruses show a decrease in numbers of lymphocytes (34). Interestingly, in this study we found NS1-GFP in hematopoietic cells, especially in DCs, monocytes ($Gr1^+$), neutrophils ($CD11b^+$), B cells, and NK cells, which are critical for controlling viral replication and development of effective adaptive immunity (35, 36). It is conceivable that highly pathogenic influenza viruses may infect high levels of these cells and/or may have preferential cellular tropism for immune cells and thereby contribute to immune deregulation and disease aggravation. Use of highly pathogenic influenza viruses expressing GFP might help to elucidate these questions in the future.

Anti-influenza drugs such as amantadine and oseltamivir are widely used for treatment of influenza-like illness (6, 7). Although the mechanism of action for these drugs has been well characterized in vitro, it is still not clear how these drugs control infection progression in vivo (4, 37–39). Here, we analyzed the effect of antiviral treatment on NS1-GFP virus infection progression. Oseltamivir treatment significantly reduced NS1-GFP virus infection in all cell types to less than 2% and restricted the NS1-GFP virus replication to localized areas (Figs. 4 and 5). Amantadine was more effective (3- to 4-fold) in preventing infection in B and NK cells, but it reduced infection only to 50% in epithelial and $CD11b^+$ $CD11c^+$ cells at the dose used (Fig. 4 *A* and *C*). Interestingly, amantadine treatment showed no effect in preventing infection of monocytes ($Gr1^+$) or neutrophils ($CD11b^+$) at later times of infection (Fig. 4 *D* and *E*). Because the ion channel activity of M2s is required for acidification of the inside of the virion during endosomal-mediated viral entry, it is possible that differences in the endosomal physiology of different cell types are responsible for these effects. Further experimentation will be required to investigate whether this is the case. Also, the levels of inflammatory monocyte and neutrophil infiltration were different in oseltamivir- and amantadine-treated mice. In oseltamivir-treated mice, the numbers of infiltrating cells were dramatically lower than in amantadine-treated mice, correlating well with the levels of antigen present in the respiratory tract. This is in agreement with

prior studies that have demonstrated that the viral load in the lungs determines the levels of immune infiltration (33).

Here, we have demonstrated the generation of a unique, fully replication-competent IAV carrying a GFP reporter gene (NS1-GFP virus). The NS1-GFP virus efficiently replicates and causes significant pathogenicity in mice. By multicolor flow-cytometric analysis, we have analyzed cell types that are GFP positive during infection. Our work provides the basis for future studies focused on understanding the consequences of infection of different cell populations. In addition, the generation of different influenza virus strains carrying a GFP reporter will allow further and more specific investigation of strain specific effects in pathogenesis, tissue tropism, and replication kinetics in different hosts in vivo. Finally, the same strategy could be adapted to generate recombinant influenza viruses carrying foreign genes in their NS segments, which can be used as a vaccines or gene therapy candidates.

Materials and Methods

Construction of NS-GFP Segment. The NS segment (A/Puerto Rico/8/34) carrying GFP was generated by overlapping fusion PCR using standard molecular biology techniques. Briefly, the NS1 ORF without the stop codon was fused to the N-terminal of a codon-optimized maxGFP (Amaxa) via a GSGG linker region (NS1-GFP). The maxGFP was followed by a short GSG linker, a 19-aa 2A autoproteolytic site (ATNFSLLKQAGDVEENPG⇓P) (12) derived from porcine teschovirus–1 and by the NEP ORF (Fig. 1*A*). Also, silent mutations in the endogenous splice acceptor site in the NS1 ORF were introduced to prevent splicing (11). The engineered NS-GFP segment was cloned in the pDZ IAV rescue plasmid (13).

Murine Experiments. All animal procedures performed in this study were conducted in accordance with Institutional Animal Care and Use Committee (IACUC) guidelines, and were approved by the IACUC of Mount Sinai School of Medicine.

Body weight loss and survival. Female BALB/c mice (5–6 wk of age) were anesthetized with ketamine–xylaxine and intranasally infected with the indicated virus dose diluted in 50 μL PBS. Body weight and survival were measured daily. Mice showing more than 25% of body weight loss were considered to have reached the experimental end point and were humanely killed.

Antiviral treatments. Mice were treated with either 50 mg/kg oseltamivir phosphate in PBS (Roche) or 40 mg/kg amantadine hydrochloride in H_2O (Sigma), administered by oral gavage (24). The treatments were started 1 h postinfection and were given once daily until the end of the experiment.

Flow Cytometry. Single-cell suspensions of mice lung were prepared using collagenase/DNase treatment. Cells were stained with commercial antibodies and analyzed using a BD LSR II flow cytometer.

More detailed descriptions of the experimental procedure are included in *SI Materials and Methods*.

ACKNOWLEDGMENTS. We thank Richard Cadagan and Osman Lizardo for invaluable and excellent technical assistance during the course of this study. We thank Donna Tscherne and Rafael Medina for critical reading of the manuscript. This work was partially supported by the Center for Research on Influenza Pathogenesis (CRIP), the National Institute of Allergy and Infectious Diseases (NIAID)–funded Center for Research in Influenza Pathogenesis (Contract HHSN266200700010C), and NIAID (Grants U19AI083025, P01AI058113, and R01AI046954).

1. Fiore AE, et al.; Centers for Disease Control and Prevention (CDC); Advisory Committee on Immunization Practices (ACIP) (2008) Prevention and control of influenza: Recommendations of the Advisory Committee on Immunization Practices (ACIP), 2008. *MMWR Recomm Rep* 57:1–60.
2. Cox NJ, Neumann G, Donis RO, Kawaoka Y (2005) Orthomyxoviruses: Influenza. *Topley and Wilson's Microbiology and Microbial Infections*, eds Mahy BWJ, ter Meulen V (Arnold, London, UK), pp 634–698.
3. Palese P, Shaw ML (2007) Orthomyxoviridae: The viruses and their replication. *Fields Virology*, eds Knipe DM, Howley PM (Lippincott Williams & Wilkins, Philadelphia, PA), 5th Ed, pp 1647–1689.
4. von Itzstein M (2007) The war against influenza: Discovery and development of sialidase inhibitors. *Nat Rev Drug Discov* 6:967–974.
5. De Clercq E (2006) Antiviral agents active against influenza A viruses. *Nat Rev Drug Discov* 5:1015–1025.
6. Hayden FG, Pavia AT (2006) Antiviral management of seasonal and pandemic influenza. *J Infect Dis* 194(Suppl 2):S119–S126.
7. Sugrue RJ, Tan BH, Yeo DS, Sutejo R (2008) Antiviral drugs for the control of pandemic influenza virus. *Ann Acad Med Singapore* 37:518–524.
8. Ibricevic A, et al. (2006) Influenza virus receptor specificity and cell tropism in mouse and human airway epithelial cells. *J Virol* 80:7469–7480.
9. Kittel C, et al. (2004) Rescue of influenza virus expressing GFP from the NS1 reading frame. *Virology* 324:67–73.
10. Shinya K, Fujii Y, Ito H, Ito T, Kawaoka Y (2004) Characterization of a neuraminidase-deficient influenza a virus as a potential gene delivery vector and a live vaccine. *J Virol* 78:3083–3088.
11. Basler CF, et al. (2001) Sequence of the 1918 pandemic influenza virus nonstructural gene (NS) segment and characterization of recombinant viruses bearing the 1918 NS genes. *Proc Natl Acad Sci USA* 98:2746–2751.
12. Donnelly ML, et al. (2001) The 'cleavage' activities of foot-and-mouth disease virus 2A site-directed mutants and naturally occurring '2A-like' sequences. *J Gen Virol* 82: 1027–1041.
13. Quinlivan M, et al. (2005) Attenuation of equine influenza viruses through truncations of the NS1 protein. *J Virol* 79:8431–8439.
14. Kochs G, García-Sastre A, Martínez-Sobrido L (2007) Multiple anti-interferon actions of the influenza A virus NS1 protein. *J Virol* 81:7011–7021.
15. García-Sastre A, et al. (1998) Influenza A virus lacking the NS1 gene replicates in interferon-deficient systems. *Virology* 252:324–330.
16. Reed LJ, Muench H (1938) A simple method of estimating fifty per cent endpoints. *Am J Hyg* 27:493–497.
17. Hao X, Kim TS, Braciale TJ (2008) Differential response of respiratory dendritic cell subsets to influenza virus infection. *J Virol* 82:4908–4919.
18. Kim TS, Braciale TJ (2009) Respiratory dendritic cell subsets differ in their capacity to support the induction of virus-specific cytotoxic CD8+ T cell responses. *PLoS ONE* 4: e4204.
19. Haye K, Burmakina S, Moran T, García-Sastre A, Fernandez-Sesma A (2009) The NS1 protein of a human influenza virus inhibits type I interferon production and the induction of antiviral responses in primary human dendritic and respiratory epithelial cells. *J Virol* 83:6849–6862.
20. López CB, Fernandez-Sesma A, Czelusniak SM, Schulman JL, Moran TM (2000) A mouse model for immunization with ex vivo virus-infected dendritic cells. *Cell Immunol* 206: 107–115.
21. Fesq H, Bacher M, Nain M, Gemsa D (1994) Programmed cell death (apoptosis) in human monocytes infected by influenza A virus. *Immunobiology* 190:175–182.
22. Seo SH, Webby R, Webster RG (2004) No apoptotic deaths and different levels of inductions of inflammatory cytokines in alveolar macrophages infected with influenza viruses. *Virology* 329:270–279.
23. Cheung CY, et al. (2002) Induction of proinflammatory cytokines in human macrophages by influenza A (H5N1) viruses: A mechanism for the unusual severity of human disease? *Lancet* 360:1831–1837.
24. Tumpey TM, et al. (2002) Existing antivirals are effective against influenza viruses with genes from the 1918 pandemic virus. *Proc Natl Acad Sci USA* 99:13849–13854.
25. Billeter MA, Naim HY, Udem SA (2009) Reverse genetics of measles virus and resulting multivalent recombinant vaccines: Applications of recombinant measles viruses. *Curr Top Microbiol Immunol* 329:129–162.
26. Pekosz A, Newby C, Bose PS, Lutz A (2009) Sialic acid recognition is a key determinant of influenza A virus tropism in murine trachea epithelial cell cultures. *Virology* 386: 61–67.
27. Scull MA, et al. (2009) Avian Influenza virus glycoproteins restrict virus replication and spread through human airway epithelium at temperatures of the proximal airways. *PLoS Pathog* 5:e1000424.
28. van Riel D, et al. (2006) H5N1 virus attachment to lower respiratory tract. *Science* 312: 399.
29. Shinya K, et al. (2006) Avian flu: Influenza virus receptors in the human airway. *Nature* 440:435–436.
30. Hashimoto Y, Moki T, Takizawa T, Shiratsuchi A, Nakanishi Y (2007) Evidence for phagocytosis of influenza virus-infected, apoptotic cells by neutrophils and macrophages in mice. *J Immunol* 178:2448–2457.
31. Tumpey TM, et al. (2004) Pathogenicity and immunogenicity of influenza viruses with genes from the 1918 pandemic virus. *Proc Natl Acad Sci USA* 101:3166–3171.
32. Tumpey TM, et al. (2005) Pathogenicity of influenza viruses with genes from the 1918 pandemic virus: Functional roles of alveolar macrophages and neutrophils in limiting virus replication and mortality in mice. *J Virol* 79:14933–14944.
33. Perrone LA, Plowden JK, García-Sastre A, Katz JM, Tumpey TM (2008) H5N1 and 1918 pandemic influenza virus infection results in early and excessive infiltration of macrophages and neutrophils in the lungs of mice. *PLoS Pathog* 4:e1000115.
34. Tumpey TM, Lu X, Morken T, Zaki SR, Katz JM (2000) Depletion of lymphocytes and diminished cytokine production in mice infected with a highly virulent influenza A (H5N1) virus isolated from humans. *J Virol* 74:6105–6116.
35. Gazit R, et al. (2006) Lethal influenza infection in the absence of the natural killer cell receptor gene Ncr1. *Nat Immunol* 7:517–523.
36. McGill J, Heusel JW, Legge KL (2009) Innate immune control and regulation of influenza virus infections. *J Leukoc Biol* 86:803–812.
37. Lew W, Chen X, Kim CU (2000) Discovery and development of GS 4104 (oseltamivir): An orally active influenza neuraminidase inhibitor. *Curr Med Chem* 7:663–672.
38. Pielak RM, Schnell JR, Chou JJ (2009) Mechanism of drug inhibition and drug resistance of influenza A M2 channel. *Proc Natl Acad Sci USA* 106:7379–7384.
39. Schnell JR, Chou JJ (2008) Structure and mechanism of the M2 proton channel of influenza A virus. *Nature* 451:591–595.

Supporting Information

Manicassamy et al. 10.1073/pnas.0914994107

SI Materials and Methods

Cell Lines. Human embryonic kidney (293T) cells were maintained in DMEM supplemented with 10% FBS and 1,000 units/mL penicillin/streptomycin. MDCK cells were maintained in MEM supplemented with 10% FBS and penicillin/streptomycin. Reagents for cell culture were purchased from Gibco Life Technologies.

Plaque Assay. MDCK cells were seeded in six-well plates, 1 d before infection, at a dilution of 10^6 cells/well. The next day, the cells were washed once with 2 mL PBS and incubated with virus diluted in 200 μL PBS containing 0.3% bovine albumin (BA) and 1,000 u/mL penicillin/streptomycin (PBS/BA; MP Biochemicals) for 1 h at 37 °C with frequent shaking. After incubation, the virus inoculum was removed and overlayed with MEM containing a 0.6% oxoid agar and 1 μg/mL L-(tosylamido-2-phenyl) ethyl chloromethyl ketone (TPCK)-treated trypsin (Sigma). The plaques were visualized by staining with Crystal Violet.

Rescue of NS1-GFP Virus. NS1-GFP virus (A/Puerto Rico/8/34 background) was rescued using standard reverse genetics techniques (1). Briefly, 0.5 μg of each of eight pDZ plasmids representing the eight segments of the IAV genome were transfected into 293T cells using Lipofectamine 2000 (Invitrogen). After 24 h, the 293T cells were resuspended in the medium, and 100 μL of the mix was injected into 8-d-old eggs. The NS1-GFP virus was harvested from the allantoic fluid at 48 hpi. The successful rescue of virus were confirmed by performing hemagglutination assay with chicken red blood cells. After plaque purification, NS1-GFP virus was amplified in 9-d-old embryonated eggs. The sequence of the NS-GFP segment in the NS1-GFP virus was confirmed by RT-PCR and sequencing. Titers of viral stocks were determined by plaque assay in MDCK cells.

Single-Cycle and Multicycle Growth Curve. MDCK cells were seeded at a dilution of 10^6 cells per well in six-well plates, 1 d before infection. The cells were washed with 2 mL PBS and incubated with 10^3 pfu virus (single-cycle) or 10^6 pfu (multicycle) virus diluted in 200 μL PBS/BA. After incubation for 1 h at 37 °C with frequent shaking, the virus inoculum was removed and 3 mL MEM containing 0.3% BA and 1 μg/mL TPCK-treated trypsin were added. At indicated times, nearly 300 μL of supernatant was removed for virus titration and was replenished with same amount of fresh medium. Viral titers were determined by plaque assay.

Immunostaining. A549 cells were infected with NS1-GFP virus at a MOI of 1. At 10 hpi, the cells were washed with PBS and fixed in 1 mL 4% formaldehyde (methanol-free) for 10 min. After permeabilization with 0.5% Triton X-100 in PBS, the cells were stained in PBS containing 2% BSA with a rabbit polyclonal anti-NP antibody. The cells were washed twice in PBS and stained with antirabbit secondary antibody conjugated to Alexa-588 (Invitrogen). Images were acquired on an Olympus XI-70 microscope at 20× using Q-Capture software.

Western Blot Analysis. MDCK cells in six-well plates were infected at a MOI of 1, and cells were lysed using 1% Triton X-100 lysis buffer (50 mM Tris-HCl, pH 7.5,150 mM NaCl, 5 mM EDTA,1% Triton X-100, and protease inhibitors) at the indicated times postinfection. The protein samples were subjected to SDS/PAGE and transferred to a polyvinylidene difluoride membrane. WT NS1 and NS1-GFP levels were assessed by immunoblotting with a rabbit polyclonal anti-NS1 antibody raised against the N-terminal 1–73 amino acids of NS1 from A/Swine/Texas/4199–2/98 (dilution 1:3,000) followed by an antirabbit secondary antibody (dilution 1:10,000) conjugated to HRP (GE Healthcare Life Sciences).

IFN-β Promoter Induction Assay. MDCK cells stably expressing firefly luciferase under the control of the human IFN-β (IFN-β) promoter were infected with a MOI of 1. At 18 hpi, the cells were washed with 2 mL PBS and lysed in 200 μL cell culture lysis reagent (Promega). The luciferase activity in 100 μL of cell lysate was measured with a firefly luciferase assay kit (Promega). Each experiment was performed in triplicate and repeated at least three times.

Murine Experiments. All animal procedures performed in this study were conducted in accordance with Institutional Animal Care and Use Committee (IACUC) guidelines, and have been approved by the IACUC of Mount Sinai School of Medicine.

Determination of LD_{50}. Female BALB/c mice (6 wk of age) were anesthetized with ketamine–xylazine and intranasally infected with PR8 or NS1-GFP virus in 50 μL at indicated doses ($n = 5$ per group). The mice were monitored daily for survival and body weight loss over a period of 14 d. Mice showing more than 25% of body weight loss were considered to have reached the experimental end point and were humanely euthanized. LD_{50} values were calculated by the method of Reed and Muench (2).

Lung titers. Lungs of infected mice were excised on days 3 and 4 postinfection and homogenized in 1 mL PBS/BA, using a mechanical homogenizer. The viral titers in the homogenates were quantified by plaque assay on MDCK cells. Each data point represents the average titer from three mice.

Lung cryosections. After surface cleaning with PBS, murine lungs were placed in OCT media and slowly frozen in −80 °C. Lung sections 5 μm in thickness were cut using a cryostat and placed on a glass slide. The sections were fixed in 200 μL PBS containing 4% formaldehyde for 10 min and washed twice with PBS. The nuclei were stained with DAPI. Images were acquired on an Olympus XI-70 microscope at 10× using Q-Capture software.

Ex vivo imaging of lungs. The lungs of infected mice were excised at the indicated times postinfection. After cleaning with PBS, the lungs were placed on a glass plate and imaged using the IVIS-200 series imaging system (Xenogen) fitted with GFP excitation/emission filters at 4-s exposure time.

Flow Cytometry. ***Single-cell preparation.*** Single-cell suspensions of mice lung were prepared using collagenase/DNase treatment. Briefly, excised whole lungs were minced in 10 mL DMEM containing 10 mM Hepes, 5% FBS, 100 units/mL Type IV Collagenase (Worthington), and 100 μg/mL DNase I (Roche), and incubated at 37 °C for 30 min. Tissue pieces were meshed through a 70-μm cell strainer. Cells were washed once with HBSS containing 10 mM Hepes buffer, 2% FBS, and 2 mM EDTA, followed by filtration using a 40-μm cell strainer. Red blood cells in the preparation were lysed using 1 mL ACK lysis buffer (Lonza). Cells were pelleted and washed once with HBSS.

Staining and analysis cell surface markers. Approximately 1×10^6 cells were stained in 100 μL HBSS (10 mM Hepes, 2% FBS, 2 mM EDTA) using commercially available antibodies in the presence of Fc receptor blocking antibody (2.4G2) for 30 min on ice. Monoclonal antibodies conjugated to different fluorochromes (PerCP-Cy5.5, APC, APC-CY7, Pacific blue, PE, PE-Cy7) were purchased from BD Biosciences and Ebioscience. Antibody clones used in cell surface staining were Fc block (2.4G2), CD45 (30-F11), CD11c (HL3), CD11b (M1/70), CD4 (GK1.5), CD8a

(53-6.7), Gr1 (RB6-8c5), B220 (RA3-6B2), Pan NK (DX5), and MHCII (M5/11.15.2). After 30 min incubation, the cells were washed twice with HBSS buffer and used directly for flow cytometry or for intracellular staining.

Intracellular staining. After staining for cell surface markers, the cells were fixed and permeabilized in 100 μL BD Cytofix/Cytoperm solution for 30 min. The cells were washed twice with BD Perm/Wash buffer and stained with anti-NP monoclonal antibody conjugated with Alexa-532 fluorphore and anti-GFP polyclonal antibody conjugated with Alexa-488 fluorophore (Evorgen). After incubation for 30 min on ice, the cells were washed three times with BD Perm/Wash buffer and once with HBSS/2% FBS buffer.

Flow cytometry was performed on a BD LSR II flow cytometer using FACSDiva software (BD Biosciences). The data were analyzed using FlowJo Software (Tree Star).

1. Fodor E, et al. (1999) Rescue of influenza A virus from recombinant DNA. *J Virol* 73: 9679–9682.

2. Reed LJ, Muench H (1938) A simple method of estimating fifty per cent endpoints. *Am J Hyg* 27:493–497.

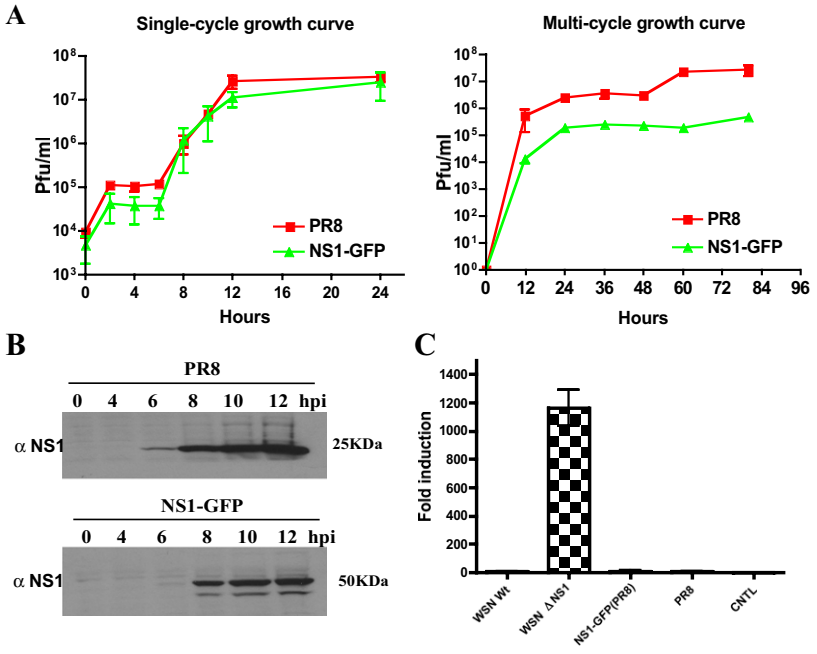

Fig. S1. In vitro characterization of NS1-GFP virus. (*A*) Single-cycle (MOI = 1) and multicyle (MOI = 0.001) growth kinetics in MDCK cells. (*B*) Western blot analysis of NS1 and NS1-GFP expression in MDCK cells. (*C*) Analysis of IFN-β promoter activation by NS1-GFP virus.

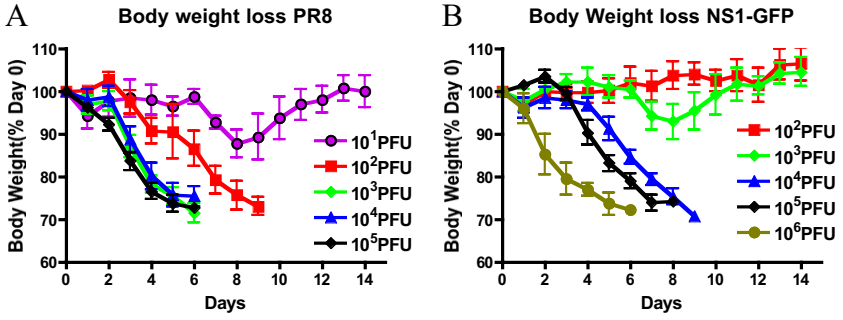

Fig. S2. In vivo characterization of NS1-GFP virus. Comparison of pathogenicity of PR8 and NS1-GFP viruses in mice. Five-wk-old female BALB/c mice were intranasally inoculated with indicated doses of PR8 (n = 5 per group) or NS1-GFP virus. Body weight was measured daily and is represented as percentage of day 0 weight.

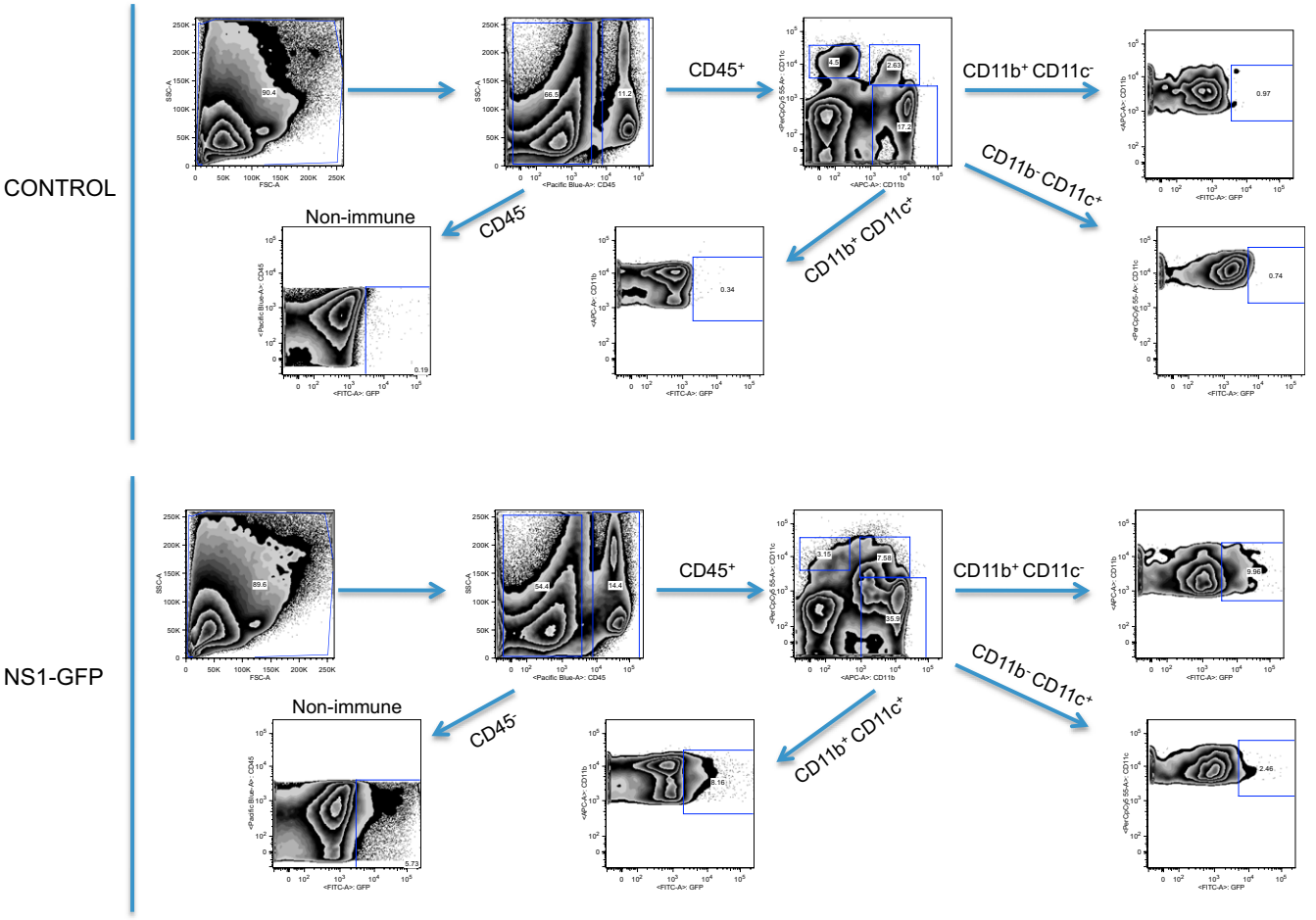

Fig. S3. Analysis of GFP expression in different APCs differentially expressing CD11b and CD11c. (*Upper*) Representative analysis of cells from control (noninfected) mice. (*Lower*) Representative analysis of cells from NS1-GFP virus–infected mice lungs at 48 hpi.

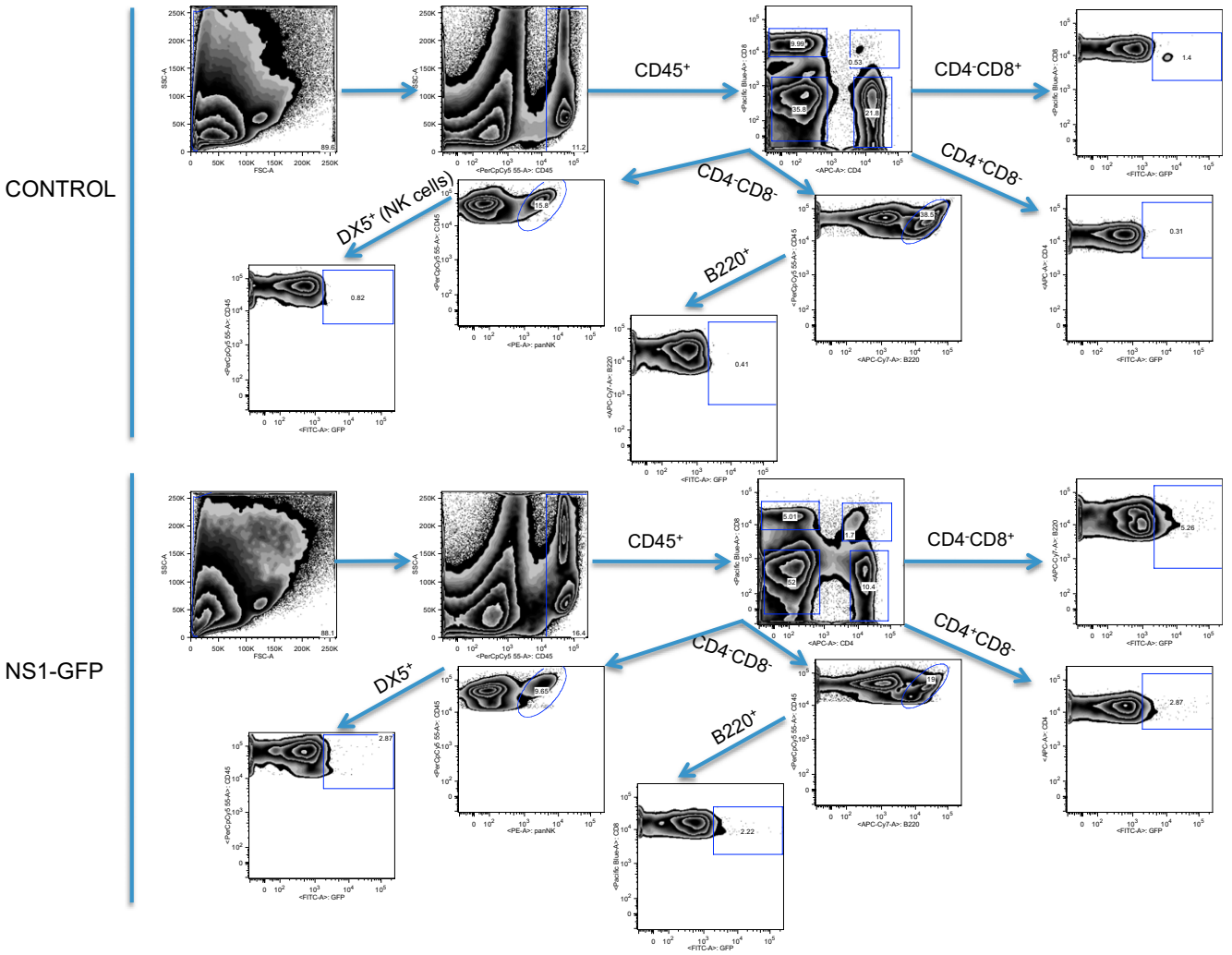

Fig. S4. Analysis of GFP expression in CD4, CD8, B, and NK cells based on cellular markers. (*Upper*) Representative analysis of cells from control (noninfected) mice. (*Lower*) Representative analysis of cells from NS1-GFP virus–infected mice lungs at 48 hpi.

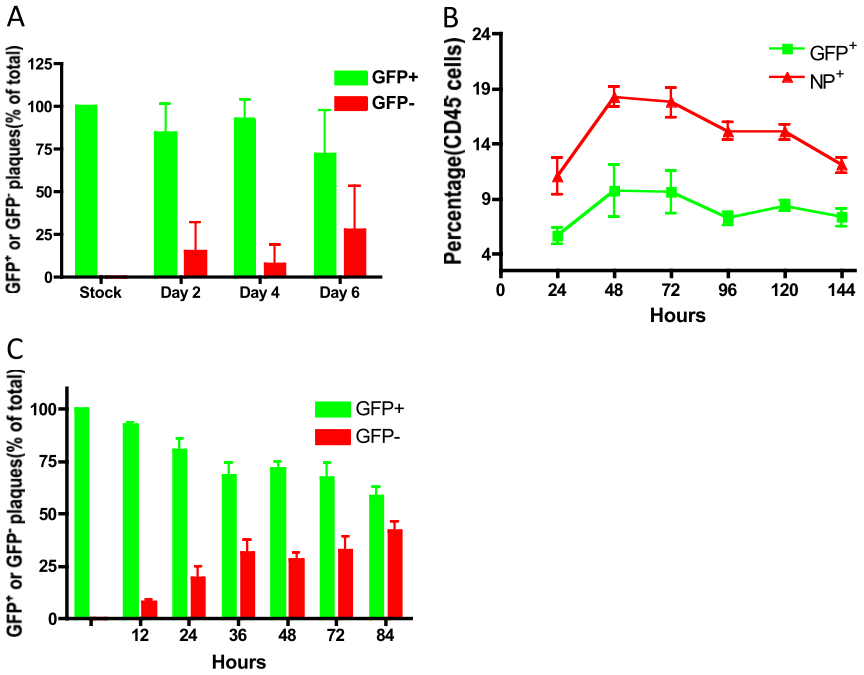

Fig. S5. Characterization of in vivo and in vitro stability of NS1-GFP virus. (*A*) Stability of NS1-GFP virus in vivo. Mice were infected with 10^4 pfu of NS1-GFP virus. Percentage of NS1-GFP carrying viruses in lung homogenates were analyzed by standard plaque assay, followed by scoring for GFP-positive or GFP-negative plaques. Each data point represents the average from at least three mice. (*B*) Kinetics of NP and GFP expression in $CD45^-$ cells from NS1-GFP virus–infected mice. Female BALB/c mice were infected with NS1-GFP virus at a dose of 10^6 pfu. Levels of NP and GFP expression in $CD45^-$ cells were analyzed using anti-NP– and anti-GFP–specific antibodies in a BD LSR II flow cytometer. Each data point represents average from at least three mice. (*C*) Stability of NS1-GFP virus in vitro. MDCK cells were infected with an MOI of 0.001. Supernantant was collected at indicated hpi and scored for levels of GFP-positive and GFP-negative plaques.